

Improved passive error correction using variable dissipation in small logical qubit architectures

David Rodríguez Pérez* and Eliot Kapit

Department of Physics, Colorado School of Mines, Golden, CO 80401 and

Department of Physics and Engineering Physics, Tulane University, New Orleans, LA 70118

Qubit coherence times for superconducting qubits have greatly improved over time. Moreover, small logical qubit architectures using engineered dissipation have shown great promise for further improvements in the coherence of a logical qubit manifold comprised of few physical qubits. Nevertheless, optimal working parameters for small logical qubits are generally not well understood. This work presents several approaches to finding preferential parameter configurations by looking at three different cases of increasing complexity. We begin by looking at state stabilization of a single qubit using dissipation via coupling to a lossy object. We look at the limiting factors in this approach to error correction, and how we address those by numerically optimizing the parametric coupling strength with the lossy object having an effective time-varying dissipation rate - we call this a pulse-reset cycle. We then translate this approach to more efficient state stabilization to an abstracted three-qubit flip code, and end by looking at the Very Small Logical Qubit (VSLQ) [1]. By using these techniques, we can further increase logical state lifetimes for different architectures. We show significant advantages in using a pulse-reset cycle over numerically optimized, fixed parameter spaces.

I. INTRODUCTION

Error correction via the encoding of logical qubits using multiple physical qubits is a very promising route towards fault-tolerant quantum computation [2]. While topological stabilizer codes like the surface code are a great way of achieving error correction, they also require many physical qubits to encode a single logical qubit. For a distance-3 surface code, one logical qubit is encoded using 17 physical qubits [2]. Concurrently, research using engineered dissipation for stabilizing quantum states has been growing [3–6]. Some prominent examples are cat codes [7–18], having already exceeded break-even [12], and the Very Small Logical Qubit (VSLQ) [1] where a logical qubit is encoded using only 4 physical qubits - coupling 2 high coherence qubits each with 2 lossy qubits or resonators.

The goal of this paper is to better characterize and understand the limiting error channels in passive error correction, and address them with a pulse-reset technique. We address this with a numerically optimized, time-parameterized coupling strength with a time-varying lossy object. In the next section, we talk about how the use of quantum noise as engineered dissipation aids in the stabilization of a quantum state, which is the fundamental mechanism by which these small logical devices achieve passive error correction. We then discuss the limiting error syndrome induced by the error correction mechanism itself, whereby the coupling strength between the high coherence and the lossy qubits may induce off-resonant transitions into unwanted leakage states. To minimize this effect, we introduce techniques borrowed from gate optimization by numerically optimizing a para-

metric, time-varying coupling strength, and qubit reset protocols that allow the lossy qubit enough time to reset as shown in Fig. 1 [19–22].

We begin by looking at the simplest, idealized scenario of a single high coherence, three level qubit device with an unwanted leakage state, coupled to a single lossy qubit or oscillator to understand the stabilization mechanism and the limiting error. The time-parameterized numerical optimization and the qubit reset protocols show a very clear advantage over a standard, fixed coupling parameter space for single qubit device state stabilization. This is done without assuming any specific architecture, the only criteria being having the ability to couple two qubit devices with strong coupling manipulation, and efficiently inducing qubit reset. To show the practicality of these techniques, we generalize its use on a three qubit flip code, in which we look at how to optimize passive correction of a qubit flip error syndrome. Having shown the improvement from using these techniques, we proceed to the more complex VSLQ, where applying these methods gives us a better performance over numerically optimizing the individual parameters in the system Hamiltonian.

II. SINGLE QUBIT STABILIZATION

A. System

For a more thorough explanation on using engineered dissipation, we direct the reader to a full review on the subject [3]. As a very simple, idealized example, we look at a case similar to [23]. Consider a single high coherence qubit device coupled to a single lossy qubit or resonator. Here, we consider the high coherence qubit device to be a three-level system with a nonlinearity δ , and the lossy resonator to be a two-level system, as shown in Fig. 2(a). For this example, our only focus is to stabilize a sin-

* drodriguezperez@mines.edu

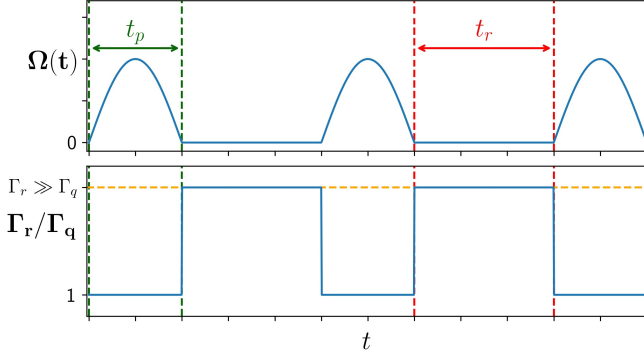


FIG. 1. Scheme for the pulse-reset cycles. We denote the coupling duration as t_p (green), in which the qubit and resonator are coupled using an optimized pulse shape. The reset cycle, t_r (red), is determined using a simple scan over different values to determine what gives the lowest residual error rate for each different T_1 . During t_p we set $\Gamma_r = \Gamma_q$ and $\Omega = \Omega_{opt}(t)$, while during t_r we have $\Gamma_r \gg \Gamma_q$ and $\Omega = 0$. It is assumed that qubit reset protocols, such as the one described in [19], can be performed efficiently, giving us an effective $\Gamma_r \gg \Gamma_q$.

gle, excited state for the high coherence qubit device in the computational basis. However, engineered dissipation can be used to stabilize an arbitrary state along any axis on the Bloch sphere, as described in [24].

We will refer to the high coherence qubit device as the primary qubit, and the ancilla as just a resonator. We can write the rotating wave Hamiltonian of this system

$$H = -\delta P_q^2 + \Omega (a_q a_r + a_q^\dagger a_r^\dagger). \quad (1)$$

Here, P_q^2 is the projector operator $|2_q\rangle\langle 2_q|$ onto the leakage state of the qubit, and Ω is the coupling strength between the qubit and resonator.

In the event of a photon loss in the qubit, $|1_q 0_r\rangle \rightarrow |0_q 0_r\rangle$, the coupled drive will excite both the qubit and resonator into their first excited states, $|0_q 0_r\rangle \rightarrow |1_q 1_r\rangle$, after which the lossiness of the resonator will bring us back to the initial desired state, $|1_q 1_r\rangle \rightarrow |1_q 0_r\rangle$. The important conditions here are: 1. $\Gamma_q \ll \Gamma_r$, meaning the lossy resonator can quickly decay back to its ground state, bringing the entire system back to the initial state $|1_q 0_r\rangle$, and; 2. $\delta \gg \Omega$, this prevents any unwanted transitions into the primary qubit leakage state induced by the coupling with the resonator. While this scheme proves very efficient in achieving passive error correction, it is the error correction mechanism itself that presents a limiting factor [25]. To that end, we explore the effects that time-parameterizing the coupling strength into pulses has on the state stabilization performance.

B. Results

Put simply, this means we let $\Omega \rightarrow \Omega_x(t), \Omega_y(t)$ as in Fig. 2(b), where

$$\Omega_{x,y}(t) = \sum_{n=1}^N c_n^{x,y} \sin(n\pi t/t_p), \quad (2)$$

and $\Omega_y(t)$ corresponds to the coupling of the term $i(a_q^\dagger a_r^\dagger - a_q a_r)$, borrowing gate optimization techniques from [26], where we use a gradient ascent numerical optimization over the $c_n^{x,y}$ coefficients for pulse shaping the time-parameterized coupling strength. By letting c_1 be some initial amplitude, and all other $c_{n \neq 1} = 0$, we find the optimized fidelity of the operation $|00\rangle \rightarrow |11\rangle$ so as to maximize the target state transition, while minimizing off-resonant transitions into the leakage state induced by the coupling itself. This is evident in Fig. 2(c), where we can see the dips in the fidelity tracking for $|10\rangle \rightarrow |10\rangle$ and $|10\rangle \rightarrow |21\rangle$ (orange and green, respectively).

In addition to optimizing the pulse shape of the coupling strength, we use alternating pulse-reset cycles in which the blue-sideband coupling strength is determined by the optimized pulse shapes during the coupling cycles. During the reset cycles, the coupling strength is completely turned off while increasing the resonator decay rate so as to allow the resonator to reset back to its ground state. This effective, induced resonator reset can be achieved with techniques described in [19]. For simplicity of simulation, we assume that this reset protocol can be achieved with high-fidelity and treat the decay rate as time-varying, which is high during the reset cycle and low during a coupling cycle (Fig. 1). The results of the residual error rate scaling using constant coupling strength versus optimized time-varying coupling strength and reset cycles are summarized in Fig. 3. While we do see a much improved scaling $\propto T_1^{-0.81}$, it is still short of the theoretical optimal $\propto T_1^{-1}$ [25]. However, given experimental limitations, this improvement is highly desirable over the asymptotically fixed coupling strength error scaling $\propto T_1^{-1/2}$, which is especially evident for short T_1 . For our comparisons, we let $T_1 \rightarrow T_1(\Omega, \Gamma_S)$, where each different T_1 has a gradient-ascent optimized parameter space.

We draw attention to the shape of the $\Omega_y(t)$ pulse that comes out of the gradient ascent search. From Fig. 4, we see that the oscillatory behaviour changes for different nonlinearity δ . Indeed, from Fig. 2(a) it is clear that having a larger nonlinearity reduces the probability for off-resonant transitions into the leakage state induced by the coupling strength. For $\delta = 2\pi \times \{200, 350\}$ MHz, we see that the frequency of this $\Omega_y(t)$ counterterm strength is exactly 200 and 350 MHz, respectively, and about 100 MHz for $\delta = 2\pi \times 100$ MHz. This opens up the possibility of a more general use of oscillatory counterterms in driven fields for state stabilization, and further research will be required to understand this phenomenon.

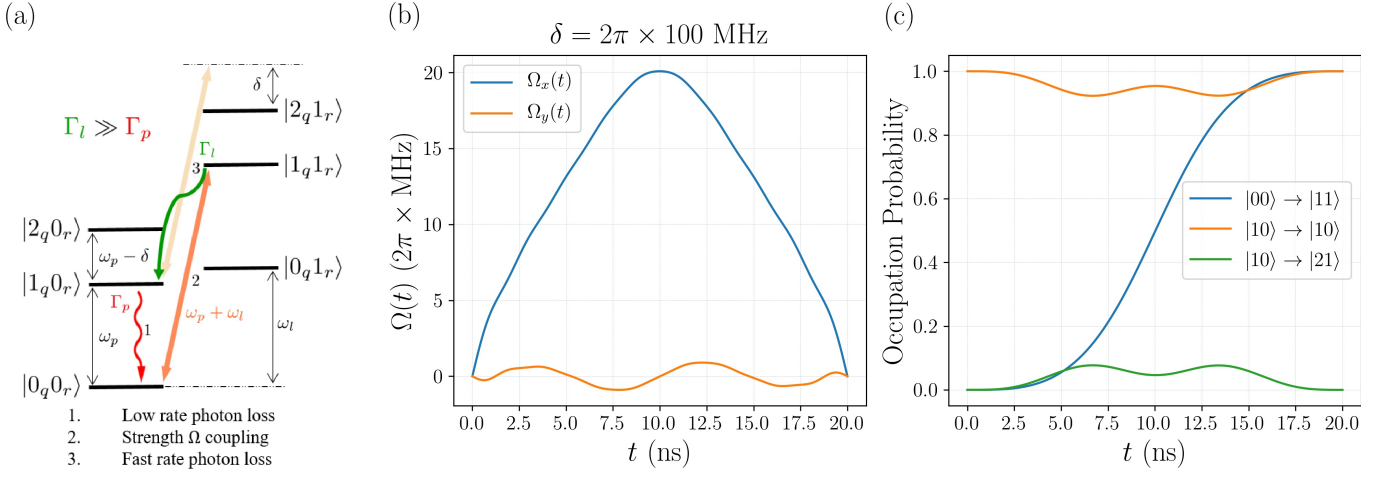


FIG. 2. A high coherence qubit coupled to a lossy qubit or resonator with a coupling strength Ω . (a) An energy level diagram of the system. The protocol follows a photon loss in the primary qubit (1), followed by the coupled excitation of both qubit and resonator at strength Ω (2), and finally the relaxation of the resonator (3). (b) Optimized pulse shape for the operation $|00\rangle \rightarrow |11\rangle$ from a gradient ascent optimization. We let $N = 20$ in Eq. 2, and initialize $c_1^x = 120$ MHz, $c_{n \neq 1}^x = 0$ MHz, and all $c_n^y = 0$, letting them vary by ϵ until we achieve a target state fidelity of 0.9989. All photon loss is turned off in this optimization, with the goal of trying to minimize errors induced by this mechanism itself. (c) We track the fidelities of the transitions $|00\rangle \rightarrow |11\rangle$ (blue), $|10\rangle \rightarrow |10\rangle$ (orange), and $|10\rangle \rightarrow |21\rangle$ (green) from the qubit-resonator coupling. The goal being to excite both qubit and resonator in the event of a photon loss, leaving the target state unchanged while minimizing off-resonant transitions into the leakage state.

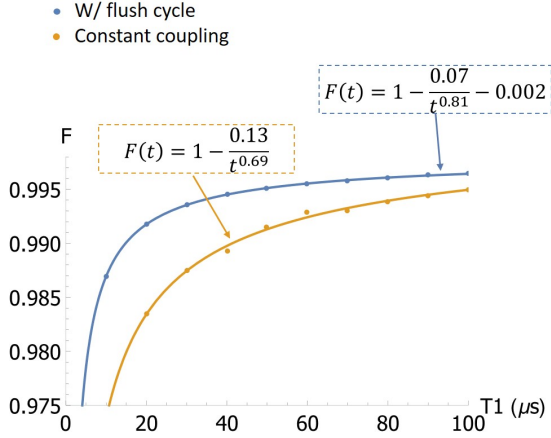


FIG. 3. Residual error rate scaling with T_1 . We use individually preferred t_r for each T_1 , and the same optimized $\Omega_{opt}(t)$ (Fig. 2(b)). We report a residual error scaling $\propto T_1^{-0.81}$, compared to $T_1^{-0.69}$ using constant coupling.

III. THREE QUBIT FLIP CODE

A. System

The single qubit case we just discussed is a very simple demonstration of the potential in using this time-parameterized technique for state stabilization. We now present the use of this technique in a more complex, yet still abstracted, system - the three qubit flip code [27]. We consider a case proposed in [28] and [29] where we

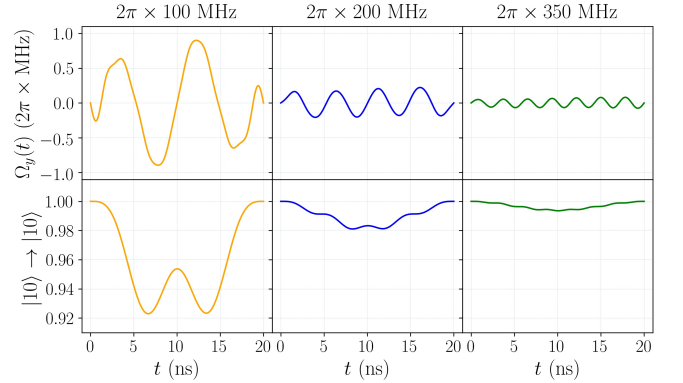


FIG. 4. The effects of the $\Omega_y(t)$ terms on off-resonant, blue-sideband transitions for $\delta = 2\pi \times \{100, 200, 350\}$ MHz. There is a clear correlation between the effective oscillating counterterm and the size of δ . This is shown by tracking the occupation of the target state $|1_q 0_r\rangle$ (bottom plots), as well as the leakage state $|2_q 1_r\rangle$ in Fig. 2(c), having initialized in the target state $|1_q 0_r\rangle$.

have 6 total qubits, three high coherence qubits each coupled to three lossy qubits, in a similar setup to [29]. We can use the Jaynes-Cummings model to describe the rotating frame Hamiltonian for this system, in which we separate the Hamiltonian into three parts for the high coherence qubits (denoted as the primary qubits Hamiltonian H_P as in [3]), the lossy resonators H_R , and the interaction Hamiltonian for the coupling between the lossy and high coherence qubits H_{PR} . We have

$$\begin{aligned}
H &= H_P + H_R + H_{PR}, \\
H_P &= -J (\sigma_{1P}^z \sigma_{2P}^z + \sigma_{2P}^z \sigma_{3P}^z + \sigma_{1P}^z \sigma_{3P}^z), \\
H_R &= -2J \sum_{i=1}^3 \sigma_{iR}^z, \quad H_{PR} = \Omega \sum_{i=1}^3 \sigma_{iP}^x (\sigma_{iR}^x + \sigma_{iR}^y),
\end{aligned} \tag{3}$$

with J being the energy scale.

Again, we look at replacing $\Omega \rightarrow \Omega(t)$ from Eq. 2, and optimizing it with a gradient ascent. This system is significantly different, however, in that it is more abstracted. Rather than trying to correct photon losses in the primary qubits, we are addressing bit flip errors. With this error syndrome, we effectively let the Lindblad operators for the system be σ^x for the primary qubits and $\{a, a^\dagger\}$ for the lossy qubits. Additionally, because we constrain the system to bit flip operations instead of ladder operators as collapse operators for the primary qubits, and to maintain a smaller Hilbert space, we only consider the computational space and ignore higher order leakage states ($|2\rangle, |3\rangle \dots$). Whereas for the single qubit system we make use of optimized coupling strength pulse shapes to perform a target operation with high fidelity while reducing induced transitions into a leakage state, here we will not have to consider the latter part. Nevertheless, there is still a non-zero probability that off-resonant flips can be induced, and so, this is a very useful example in demonstrating passive, high fidelity, time parameterized coupling strength for error correction.

While the idea is exactly the same as the single qubit stabilization, there are some things to keep in mind that change the outcome of our goal. For this particular system, we are not trying to stabilize a single state but rather a logical manifold. Namely,

$$|0_L\rangle \equiv |000\rangle, \quad |1_L\rangle \equiv |111\rangle$$

where in the flip code, the logical states are protected against individual qubit errors by following the majority vote ($|100\rangle \equiv |0_L\rangle$ and $|011\rangle \equiv |1_L\rangle$). Two flip errors on physical qubits is a logical flip error. The goal of applying this lossy coupling technique is, therefore, to protect the logical states by passively undoing flip errors corresponding to the appropriate parent logical state. So we can't simply just flip any $|0\rangle$ states to $|1\rangle$, rather the target operations for $\Omega_x(t)$ and $\Omega_y(t)$ would be

$$\begin{aligned}
|100\rangle_P \otimes |000\rangle_R &\rightarrow |000\rangle_P \otimes |100\rangle_R \\
|101\rangle_P \otimes |000\rangle_R &\rightarrow |111\rangle_P \otimes |010\rangle_R,
\end{aligned} \tag{4}$$

where our time-dependent interaction Hamiltonian would be

$$H_{PR} = \sum_{i=1}^3 \sigma_{iP}^x (\Omega_x(t) \sigma_{iR}^x + \Omega_y(t) \sigma_{iR}^y). \tag{5}$$

Note from Eq. 4 that these operations are achieved by the red- and blue-sideband couplings described in [24, 30].

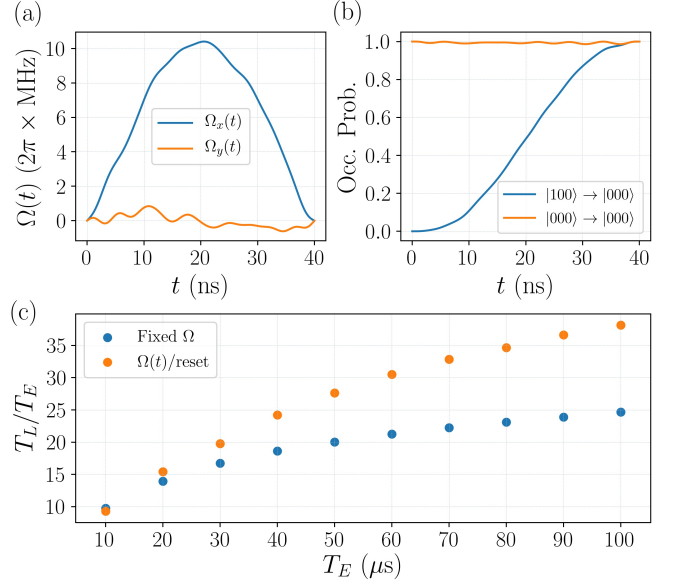


FIG. 5. Results for the three qubit code using $J = 2\pi \times 20$ MHz and $\Gamma_R = 30$ MHz. The optimized pulse shape for the target operations in Eq. 4(a), as well as tracking the operation fidelity (b). Note that the states in the legend are only the primary qubits subspace. (c) Improvement factor T_L/T_E for the states $|000\rangle_P$ and $|111\rangle_P$, with increasing error times T_E .

We emphasize that like the single qubit stabilization example, this system is still idealized and abstracted. A more thorough characterization that includes leakage states would be needed for a more realistic demonstration of using a pulse-reset evolution with a qubit flip error syndrome. However, as we saw for the single qubit, it is safe to assume that with a large enough nonlinearity, and with the oscillating $\Omega_y(t)$ counterterm having numerically optimized a time-parameterized coupling strength, we can reasonably exclude leakage transitions from our simulations.

B. Results

We summarize the results for this system in Fig. 5. The $\Omega_y(t)$ pulse shape in Fig. 5(top left) does not have the same oscillatory behavior as we saw for the single qubit, which is consistent with our exclusion of a leakage state and thus no nonlinearity to correlate to. Instead, we see a pulse shape that is somewhat proportional to the time derivative of the $\Omega_x(t)$ term, which is consistent with what we would expect from the DRAG protocol in gate optimization techniques [26]. While there are still unwanted transitions out of the target logical state $|000\rangle$ during the pulse evolution, seen in Fig. 5(top right), we still see a very good target operation (Eq. 4) fidelity of $1 - F < 10^{-6}$. The lifetime improvement for the states $|000\rangle_P$ and $|111\rangle_P$ has a much better scaling for increasing error times T_E , seen in Fig. 5(bottom). This is still

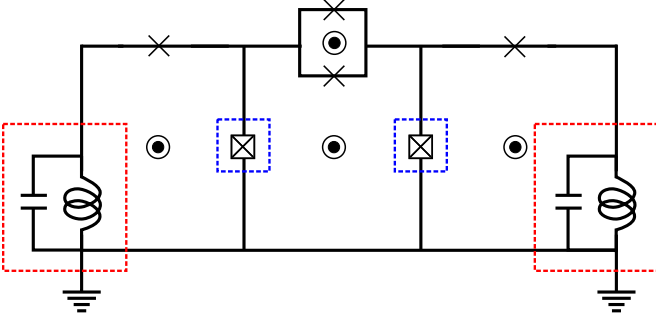


FIG. 6. A possible implementation of the logical qubit, similar to [1]. The high coherence primary qubits are in blue boxes, and the lossy resonators (or qubits) are in red boxes. The rotating wave Hamiltonian (Eq. 6) achieved by modulating the flux drives in the diagram. We refer to the elements of this circuit as shadow left and shadow right (Sl and Sr respectively) for the lossy resonators, and simply left and right (l and r) for the primary qubits.

not a linear scaling, indicative that there are other residual error rates that become dominant for larger T_E , but the improvement is very significant over using individually optimized fixed coupling strengths.

IV. VSLQ

A simple yet effective architecture, the VSLQ shows great promise in protecting a logical state against single photon loss errors while suppressing phase errors, all while depending on fully available technology. Having shown the applicability of this pulse-reset technique on a more complicated system, we now apply it to a more realistic implementation, the VSLQ [1, 3].

A. System

This circuit consists of two coupled high coherence qubits each coupled to a lossy qubit or resonator, as shown in Fig. 6. Following the derivation of the rotating wave Hamiltonian from [1], and using the same notation, we have $H = H_P + H_S + H_{PS}$, with

$$\begin{aligned} H_P &= -W \tilde{X}_l \tilde{X}_r + \frac{\delta}{2} (P_l^1 + P_r^1) \\ H_S &= \left(W + \frac{\delta}{2} \right) (a_{Sl}^\dagger a_{Sl} + a_{Sr}^\dagger a_{Sr}) \\ H_{PS} &= \Omega (a_l^\dagger a_{Sl}^\dagger + a_r^\dagger a_{Sr}^\dagger + \text{H.c.}), \end{aligned} \quad (6)$$

where δ is a nonlinearity, $\tilde{X}_k = (a_k^\dagger a_k^\dagger + a_k a_k) / \sqrt{2}$, and $P_k^n = |n_k\rangle\langle n_k|$, $k = \{l, r\}$. Here H_P denotes the Hamiltonian for the primary qubits, where we only consider the first three levels as the operating space and ignore higher

order states ($|3\rangle, |4\rangle, \dots$) so as to reduce the size of the Hilbert space and ease numerical simulations. H_S is the Hamiltonian for the "shadow" resonators (blue and red respectively in Fig. 6), with H_{PS} the interaction Hamiltonian.

Using the eigenstates for Eq. 6, we can define a logical manifold:

$$\begin{aligned} |0_L\rangle &= \frac{1}{\sqrt{2}} (|0_l\rangle + |2_l\rangle) \otimes \frac{1}{\sqrt{2}} (|0_r\rangle + |2_r\rangle) \otimes |0_{Sl}0_{Sr}\rangle \\ |1_L\rangle &= \frac{1}{\sqrt{2}} (|0_l\rangle - |2_l\rangle) \otimes \frac{1}{\sqrt{2}} (|0_r\rangle - |2_r\rangle) \otimes |0_{Sl}0_{Sr}\rangle. \end{aligned} \quad (7)$$

These states are passively protected against single-photon losses by the blue-sideband coupling in H_{PS} , which is only energetically preferred in the event of a photon loss in one of the primary qubits, leading to long lifetimes of the logical states. This is very similar the blue-sideband coupling for the single qubit case shown in Fig. 2(a). A major difference here is that instead of trying to stabilize a single excited state, the goal is to stabilize these superposition states. So while a single photon loss can take the system out of the logical manifold into an error state

$$|\text{Err}_l\rangle = |1_l\rangle \otimes \frac{1}{\sqrt{2}} (|0_r\rangle \pm |2_r\rangle) \otimes |0_{Sl}0_{Sr}\rangle, \quad (8)$$

transitions into this same exact state can be induced by H_{PS} . In addition to attempting to minimize these unwanted transitions by $\Omega(t)$, we also need to consider transitions into a higher order terms. This could make the \tilde{X} terms in H_P maintain a state in the superposition $|2\rangle + |4\rangle$, which would be a corresponding leakage state. Moreover, accounting for higher excited states means that we also must consider the possibility of the \tilde{X} terms taking an error state $|1\rangle$ and taking it to a superposition $|1\rangle + |3\rangle$. However, given that such off-resonant transitions are extremely unlikely due to increasing nonlinearities with increasing energy, for these simulations we limit the primary qubits to three level systems, and try to address the much higher probability transition $|0\rangle + |2\rangle \rightarrow |1\rangle$. We assume that it is significantly more likely this error state will be corrected as opposed to finding a higher order state.

The optimized pulse shape will correspond to the interaction Hamiltonian

$$\begin{aligned} H_{PS} &= \Omega_x(t) (a_l^\dagger a_{Sl}^\dagger + a_r^\dagger a_{Sr}^\dagger + \text{H.c.}) \\ &\quad + \Omega_y(t) i (a_l^\dagger a_{Sl}^\dagger + a_r^\dagger a_{Sr}^\dagger - \text{H.c.}), \end{aligned}$$

just like we did for the single and three qubit cases, with the same goal of having this pulse shape reduce changes to our target logical states Eq. 7 and achieving the target operation

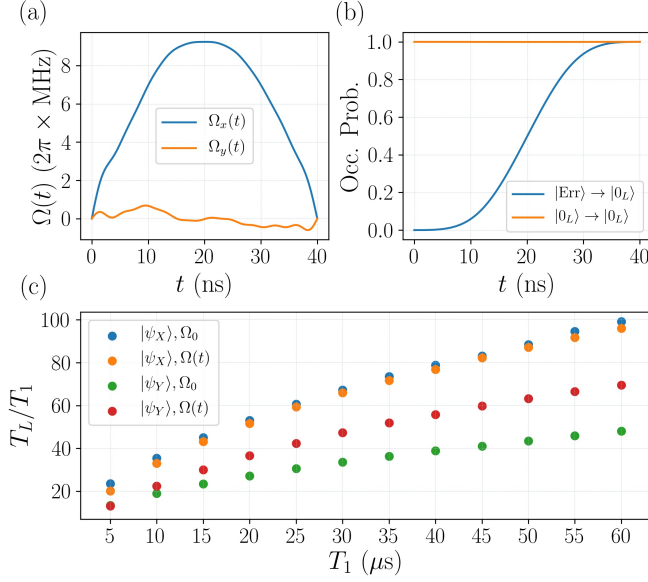


FIG. 7. Results for the VSLQ. (a) Optimized $\Omega_x(t)$ and $\Omega_y(t)$ pulse shapes. Again, we see $\Omega_y(t) \propto \frac{d}{dt}\Omega_x(t)$, giving us a high fidelity target operation while leaving the target states unchanged (b). We see the effects of lifetimes for X_L eigenstates and Y_L eigenstates (c), using definitions from [1]. Blue and green are the improvement factors using fixed operating parameters (Table. I) for the X_L and Y_L eigenstates, respectively, while orange and red are the improvement factors using pulse-reset cycles.

$$\begin{aligned}
 &|1_L\rangle \otimes \frac{1}{\sqrt{2}}(|0_r\rangle \pm |2_r\rangle) \otimes |0_{Sl}0_{Sr}\rangle \\
 &\rightarrow \frac{1}{\sqrt{2}}(|0_L\rangle + |2_L\rangle) \otimes \frac{1}{\sqrt{2}}(|0_r\rangle + |2_r\rangle) \otimes |1_{Sl}0_{Sr}\rangle
 \end{aligned}$$

with high fidelity. During the reset cycle, where $\Gamma_S \gg \Gamma_P$, the lossy qubit returns to its ground state $|1_{Sl}0_{Sr}\rangle \rightarrow |0_{Sl}0_{Sr}\rangle$, we are back to the logical manifold Eq. 7.

B. Results

These results using pulse-reset cycles are summarized in Fig. 7, we compare these to results from running a gradient ascent over the fixed parameter space $\{\Omega, \omega_S, \Gamma_S\}$, summarized in Table. I. These fixed parameter results are our benchmark in looking for an improvement from our pulse-reset protocol.

Using the optimized pulse shapes for $\Omega_x(t)$ and $\Omega_y(t)$ from Fig. 7(top left), we achieve an operation fidelity of $1 - F < 10^{-4}$, without any noticeable transitions out of the target state $|0_L\rangle$ (Fig. 7(top right)). We can see that this technique does not show an improvement for the long-time X_L eigenstate lifetimes over using individually, optimized fixed parameters (Fig. 7(bottom)). However, the improvement in the lifetimes for the Y_L eigenstates is

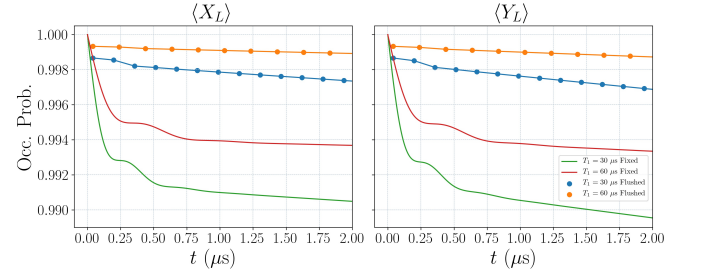


FIG. 8. Short time evolution for the VSLQ X_L eigenstates (left) and Y_L eigenstates (right). We compare using fixed parameters from Table. I versus using pulse-reset (flushed) cycles for $T_1 = 30, 60 \mu\text{s}$.

TABLE I. Gradient ascent results over the fixed parameter space of the VSLQ with $W = 2\pi \times 35 \text{ MHz}$, and $\delta = 2\pi \times 350 \text{ MHz}$. Note the lossy qubit energy approaches the energy from Eq. 6, $\omega_S = W + \delta/2 = 2\pi \times 210 \text{ MHz}$.

T_1 μs	Ω $2\pi \times \text{MHz}$	Γ_S MHz	ω_S $2\pi \times \text{MHz}$	T_X μs	T_Y μs
5	2.94	24.66	209.75	117	66
10	2.15	18.40	209.83	353	189
15	1.81	15.32	209.90	675	350
20	1.59	13.26	209.92	1061	542
25	1.43	12.09	209.94	1514	762
30	1.31	11.09	209.95	2016	1005
35	1.22	10.30	209.96	2571	1271
40	1.14	9.67	209.96	3151	1553
45	1.08	9.15	209.96	3743	1846
50	1.02	8.73	209.97	4422	2168
55	0.98	8.38	209.97	5207	2524
60	0.93	8.04	209.97	5955	2879

very evident. Moreover, the pulse-reset evolution shows a significant improvement over fixed parameters for short time evolutions, as shown in Fig. 8. Here, we see that for both X_L and Y_L eigenstates, there is a very noticeable advantage, which will prove significantly important for gate operations on the device. In using $\Omega(t)$, we also scan over different reset times for each T_1 , since each will have a different probability of having a photon in the lossy qubit after the pulse duration $t_p = 40 \text{ ns}$. The loss rate for this lossy qubit is $\Gamma_S = 35 \text{ MHz}$ for all different T_1 during the reset cycle, and again, $\Gamma_S = \Gamma_P$ during the pulse cycles.

A lack of improvement for the VSLQ logical state lifetimes using this pulse-reset is indicative of not accounting for different error channels. This is not the case for the Y_L eigenstates, where we use the definitions from [1] to define $Y_L = iX_L Z_L$, with $X_L = \tilde{X}_L$ or \tilde{X}_R , and $Z_L = \tilde{Z}_L \tilde{Z}_R$ with $\tilde{Z}_k = P_k^2 - P_k^0$. We see in Fig. 7(bottom) that there is a clear advantage in the Y_L lifetimes using pulse-reset cycles over fixed operating parameters. While we still expected to see an advantage for the X_L eigenstates as well, we may be seeing these results because the Y_L eigenstates are sensitive to more error channels than the X_L

eigenstates.

To see this more clearly, consider the X_L eigenstate $|0_L\rangle$ from Eq. 7 undergoing a photon loss in the left qubit, taking the system to the error state Eq. 8. As previously explained, this state can then either be corrected back to the logical manifold, or undergo a second photon loss with lower probability on either qubit. In the event of a second photon loss occurring in the right qubit, then the system will be taken to the $|1_l 1_r 0_{Sl} 0_{Sr}\rangle$ state, which is uncorrectable with passive error correction having lost all information from the original state. This is considered a leakage state for the VSLQ. However, if the second photon loss occurs in the left qubit, then this can take the system to either state:

$$|\psi_1\rangle = \frac{1}{\sqrt{2}}(|0_l\rangle - |2_l\rangle) \otimes \frac{1}{\sqrt{2}}(|0_r\rangle + |2_r\rangle) \otimes |0_{Sl} 0_{Sr}\rangle, \text{ or}$$

$$|\psi_2\rangle = \frac{1}{\sqrt{2}}(|0_l\rangle + |2_l\rangle) \otimes \frac{1}{\sqrt{2}}(|0_r\rangle + |2_r\rangle) \otimes |0_{Sl} 0_{Sr}\rangle.$$

Having started in $|0_L\rangle$, the first possible outcome from a second loss in the left qubit is an error for any state, while the second is just $|0_L\rangle$, and is therefore not seen as an X_L eigenstate error. However, this last photon loss channel is an error channel for a Y_L eigenstate. And so, this may be why using an optimized target operation for this passive mechanism shows a significant improvement in the Y_L lifetimes, but not for the X_L lifetimes.

A more thorough understanding of the error channels experienced by this system and occupation of higher order states will be needed for future studies. Nevertheless, we note that the short time performance of the pulse-reset evolution still outperforms a fixed parameter evolution for any state, as seen in Fig. 8. This suggests a very practical use case for short time applications. Implementing dissipative engineering in digital error correction codes is a very attractive prospect, where in the case of the Surface Code, each error correction cycle consists of repeated measurement and resetting in short time periods. Using the advantage in the short time behavior of the pulse-reset cycle, and a proposed scheme for gates in small logical qubits ([31]), would provide a very relevant improvement in gate fidelity and error detection by incorporating small logical qubits with digital codes. This suggests a much more dramatic improvement in long term error correction than is suggested in Fig. 7. Exploring this further will be the focus of future work.

V. CONCLUSION

We have demonstrated the use of time-parameterized coupling strength and time-varying loss rates in engineered dissipation for higher fidelity state stabilization

using alternating pulse cycles and reset times as shown in Fig. 1. This showed very noticeable advantages for an idealized single qubit stabilization scheme and for a more complex bit-flip error correction code. However, for the VSLQ we saw a mixture of results, where the pulse-reset evolutions showed very clear advantage for the VSLQ eigenstates over short time evolutions, while not so much for the long-time evolutions of the VSLQ's X_L eigenstates. Moreover, we did see a clear advantage in prolonging the logical lifetimes of Y_L eigenstates, all of which is a great showcase for the use of this technique for a promising architecture, especially with gate implementations.

Nevertheless, while using passive error correction achieves significantly longer lifetimes over their component qubits for superconducting architectures, it comes at the cost of increasing complexity. This is something that will need to be carefully characterized for further implementations of small logical qubits in larger quantum computing systems, since physically implementing 2-qubit gates for small logical qubits will in itself be a complex task. However, as mentioned above, using numerical pulse-shaping for optimized targeted operations could be used to convert leakage errors into logical errors, which are then correctable with dissipative engineering. In the example of the VSLQ, having a leakage state $|1_l 1_r 0_{Sl} 0_{Sr}\rangle$ is uncorrectable for passive error correction using fixed operating parameters. Using a pulse-reset technique with time-varying coupling optimized to perform a target operation taking either qubit from $|1\rangle$ to $|0\rangle + |2\rangle$, it has the potential to be used for correcting $|1_l 1_r 0_{Sl} 0_{Sr}\rangle$. This ability to induce transitions from a leakage error state to an ordinary logical error state is a key function if ever implementing small logical qubits in digital error correction codes.

Further research will be needed to fully understand other prevalent error channels for small logical qubit architectures - especially those involving higher order states in primary high coherence qubit devices - as well as limitations of this pulse-reset technique. We would also like to explore if this technique would provide any sort of advantage in gates for small logical qubits [31], an important characterization for further implementation of these qubits towards fault-tolerance.

VI. ACKNOWLEDGEMENTS

We'd like to thank Nick Materise and Zhijie Tang for the many conversations that helped advance this project. This work was supported by the NSF grant (PHY-1653820) and ARO grant No. W911NF-18-1-0125. It was made possible by the high performance computing resources from the Tulane University Cypress platform, and the Colorado School of Mines Wendian platform.

-
- [1] E. Kapit, Hardware-Efficient and Fully Autonomous Quantum Error Correction in Superconducting Circuits, *Physical Review Letters* **116**, 150501 (2016).
- [2] A. G. Fowler, M. Mariantoni, J. M. Martinis, and A. N. Cleland, Surface codes: Towards practical large-scale quantum computation, *Physical Review A - Atomic, Molecular, and Optical Physics* **86**, 10.1103/PhysRevA.86.032324 (2012).
- [3] E. Kapit, The upside of noise: engineered dissipation as a resource in superconducting circuits, *Quantum Science and Technology* **2**, 033002 (2017).
- [4] Y. Ma, Y. Xu, X. Mu, W. Cai, L. Hu, W. Wang, X. Pan, H. Wang, Y. P. Song, C. L. Zou, and L. Sun, Error-transparent operations on a logical qubit protected by quantum error correction, (2019), arXiv:1909.06803.
- [5] J. M. Gertler, B. Baker, J. Li, S. Shirol, J. Koch, and C. Wang, Protecting a Bosonic Qubit with Autonomous Quantum Error Correction, (2020), arXiv:2004.09322.
- [6] L. B. Kristensen, M. Kjaergaard, C. K. Andersen, and N. T. Zinner, Hybrid Quantum Error Correction in Qubit Architectures, (2019), arXiv:1909.09112.
- [7] Z. Leghtas, G. Kirchmair, B. Vlastakis, R. J. Schoelkopf, M. H. Devoret, and M. Mirrahimi, Hardware-Efficient Autonomous Quantum Memory Protection, *Physical Review Letters* **111**, 120501 (2013).
- [8] M. Mirrahimi, Z. Leghtas, V. V. Albert, S. Touzard, R. J. Schoelkopf, L. Jiang, and M. H. Devoret, Dynamically protected cat-qubits: a new paradigm for universal quantum computation, *New Journal of Physics* **16**, 045014 (2014).
- [9] L. Sun, A. Petrenko, Z. Leghtas, B. Vlastakis, G. Kirchmair, K. M. Sliwa, A. Narla, M. Hatridge, S. Shankar, J. Blumoff, L. Frunzio, M. Mirrahimi, M. H. Devoret, and R. J. Schoelkopf, Tracking photon jumps with repeated quantum non-demolition parity measurements, *Nature* **511**, 444 (2014).
- [10] Z. Leghtas, S. Touzard, I. M. Pop, A. Kou, B. Vlastakis, A. Petrenko, K. M. Sliwa, A. Narla, S. Shankar, M. J. Hatridge, M. Reagor, L. Frunzio, R. J. Schoelkopf, M. Mirrahimi, and M. H. Devoret, Quantum engineering. Confining the state of light to a quantum manifold by engineered two-photon loss., *Science (New York, N.Y.)* **347**, 853 (2015).
- [11] V. V. Albert, C. Shu, S. Krastanov, C. Shen, R.-B. Liu, Z.-B. Yang, R. J. Schoelkopf, M. Mirrahimi, M. H. Devoret, and L. Jiang, Holonomic Quantum Control with Continuous Variable Systems, *Physical Review Letters* **116**, 140502 (2016).
- [12] N. Ofek, A. Petrenko, R. Heeres, P. Reinhold, Z. Leghtas, B. Vlastakis, Y. Liu, L. Frunzio, S. M. Girvin, L. Jiang, M. Mirrahimi, M. H. Devoret, and R. J. Schoelkopf, Extending the lifetime of a quantum bit with error correction in superconducting circuits, *Nature* **536**, 441 (2016).
- [13] J. Cohen, W. C. Smith, M. H. Devoret, and M. Mirrahimi, Degeneracy-Preserving Quantum Nondemolition Measurement of Parity-Type Observables for Cat Qubits, *Physical Review Letters* **119**, 060503 (2017).
- [14] S. O. Mundhada, A. Grimm, S. Touzard, U. Vool, S. Shankar, M. H. Devoret, and M. Mirrahimi, Generating higher-order quantum dissipation from lower-order parametric processes, *Quantum Science and Technology* **2**, 024005 (2017).
- [15] M. H. Michael, M. Silveri, R. Brierley, V. V. Albert, J. Salmilehto, L. Jiang, and S. Girvin, New Class of Quantum Error-Correcting Codes for a Bosonic Mode, *Physical Review X* **6**, 031006 (2016).
- [16] C. Wang, Y. Y. Gao, P. Reinhold, R. W. Heeres, N. Ofek, K. Chou, C. Axline, M. Reagor, J. Blumoff, K. M. Sliwa, L. Frunzio, S. M. Girvin, L. Jiang, M. Mirrahimi, M. H. Devoret, and R. J. Schoelkopf, A Schrödinger cat living in two boxes., *Science (New York, N.Y.)* **352**, 1087 (2016).
- [17] R. W. Heeres, P. Reinhold, N. Ofek, L. Frunzio, L. Jiang, M. H. Devoret, and R. J. Schoelkopf, Implementing a universal gate set on a logical qubit encoded in an oscillator, *Nature Communications* **8**, 94 (2017).
- [18] S. Puri, S. Boutin, and A. Blais, Engineering the quantum states of light in a Kerr-nonlinear resonator by two-photon driving, *npj Quantum Information* **3**, 18 (2017).
- [19] P. Magnard, P. Kurpiers, B. Royer, T. Walter, J. C. Besse, S. Gasparinetti, M. Pechal, J. Heinsoo, S. Storz, A. Blais, and A. Wallraff, Fast and Unconditional All-Microwave Reset of a Superconducting Qubit, *Physical Review Letters* **121**, 10.1103/PhysRevLett.121.060502 (2018).
- [20] M. D. Reed, B. R. Johnson, A. A. Houck, L. Dicarlo, J. M. Chow, D. I. Schuster, L. Frunzio, and R. J. Schoelkopf, Fast reset and suppressing spontaneous emission of a superconducting qubit, *Applied Physics Letters* **96**, 203110 (2010), arXiv:1003.0142.
- [21] S. O. Valenzuela, W. D. Oliver, D. M. Berns, K. K. Berggren, L. S. Levitov, and T. P. Orlando, Microwave-induced cooling of a superconducting qubit, *Science* **314**, 1589 (2006).
- [22] K. Geerlings, Z. Leghtas, I. M. Pop, S. Shankar, L. Frunzio, R. J. Schoelkopf, M. Mirrahimi, and M. H. Devoret, Demonstrating a driven reset protocol for a superconducting qubit, *Physical Review Letters* **110**, 120501 (2013), arXiv:1211.0491.
- [23] Y. Lu, S. Chakram, N. Leung, N. Earnest, R. K. Naik, Z. Huang, P. Groszkowski, E. Kapit, J. Koch, and D. I. Schuster, Universal Stabilization of a Parametrically Coupled Qubit, *Physical Review Letters* **119**, 10.1103/PhysRevLett.119.150502 (2017).
- [24] Z. Huang, Y. Lu, E. Kapit, D. I. Schuster, and J. Koch, Universal stabilization of single-qubit states using a tunable coupler, *Physical Review A* **97**, 1 (2018), arXiv:1803.01079.
- [25] R. Ma, C. Owens, A. Houck, D. I. Schuster, and J. Simon, Autonomous stabilizer for incompressible photon fluids and solids, *Physical Review A* **95**, 10.1103/PhysRevA.95.043811 (2017).
- [26] F. Motzoi, J. M. Gambetta, P. Rebentrost, and F. K. Wilhelm, Simple Pulses for Elimination of Leakage in Weakly Nonlinear Qubits, *Physical Review Letters* **103**, 10.1103/PhysRevLett.103.110501 (2009).
- [27] M. D. Reed, L. DiCarlo, S. E. Nigg, L. Sun, L. Frunzio, S. M. Girvin, and R. J. Schoelkopf, Realization of three-qubit quantum error correction with superconducting circuits, *Nature* **482**, 382 (2012).
- [28] J. Cohen and M. Mirrahimi, Dissipation-induced continuous quantum error correction for superconducting circuits, *Physical Review A* **90**, 062344 (2014).

- [29] E. Kapit, M. Hafezi, and S. H. Simon, Induced Self-Stabilization in Fractional Quantum Hall States of Light, *Physical Review X* **4**, 031039 (2014).
- [30] E. Kapit, Universal two-qubit interactions, measurement, and cooling for quantum simulation and computing, *Physical Review A - Atomic, Molecular, and Optical Physics* **92**, 012302 (2015), arXiv:1502.02684.
- [31] E. Kapit, Error-Transparent Quantum Gates for Small Logical Qubit Architectures, *Physical Review Letters* **120**, 50503 (2018).